



Contents lists available at ScienceDirect

## Composites Part B

journal homepage: [www.elsevier.com/locate/compositesb](http://www.elsevier.com/locate/compositesb)

# Large-strain poroelastic plate theory for polymer gels with applications to swelling-induced morphing of composite plates

Alessandro Lucantonio <sup>a,\*</sup>, Giuseppe Tomassetti <sup>b</sup>, Antonio DeSimone <sup>a</sup><sup>a</sup> SISSA - International School for Advanced Studies, Via Bonomea 265, 34136 Trieste, Italy<sup>b</sup> Dipartimento di Ingegneria Civile e Ingegneria Informatica, Università degli Studi di Roma "Tor Vergata", Via Politecnico 1, 00133 Roma, Italy

## ARTICLE INFO

## Article history:

Received 9 July 2016

Received in revised form

17 September 2016

Accepted 20 September 2016

Available online xxx

## Keywords:

Plates

Large strain

Polymer gel

Swelling

## ABSTRACT

We derive a large-strain plate model that allows to describe transient, coupled processes involving elasticity and solvent migration, by performing a dimensional reduction of a three-dimensional poroelastic theory. We apply the model to polymer gel plates, for which a specific kinematic constraint and constitutive relations hold. Finally, we assess the accuracy of the plate model with respect to the parent three-dimensional model through two numerical benchmarks, solved by means of the finite element method. Our results show that the theory offers an efficient computational framework for the study of swelling-induced morphing of composite gel plates.

© 2016 Elsevier Ltd. All rights reserved.

## 1. Introduction

The analysis of plates and shells undergoing large strains has attracted a considerable research effort, especially in computational mechanics [1–5]. So far, attention has been essentially restricted to hyperelastic and viscoelastic materials, including rubber-like materials. On the other hand, in the context of thin elastic structures consisting of polymer gels, where rubber-like elasticity is coupled with the motion of a fluid that causes the material to swell, large-strain poroelastic plate models are needed. The complexity of current theories of polymer gel swelling [6–8] stems from their non-linear, multiphysics and three-dimensional character and typically demands for computationally intensive numerical solutions [9–11]. In partial response to these issues, the formulation of dimensionally-reduced theories, including poroelastic plate theories [12], will allow to develop efficient computational models, and occasionally to gain insight from analytical or semi-analytical solutions, which are seldom found for three-dimensional models.

In this spirit but in a different context, a number of plate and shell models has been developed in recent years to describe the mechanics of thin elastic bodies undergoing material growth

[13–15]. These models were mainly motivated by the study of shape formation and mechanical instabilities in natural and biological thin structures [16]. Later, these theories have been applied to model shape morphing of responsive gels by regarding swelling as the result of growth [17,18] or distortion [19–21]. Specifically, in such applications, photolithographic patterning of the cross-linking density of thin gel membranes [22–24] and, more generally, fabrication of composite thin gel structures enable three-dimensional transformations through non-homogeneous or anisotropic swelling. Despite their success in reproducing experimental results, these models do not include any thermodynamic treatment of swelling and, as a result, they lack the relation between elasticity of the network and degree of swelling. Such relation is usually introduced phenomenologically through experimental calibration. Finally, all the proposed growth-based models lack an evolution structure, since they do not include the balance of solvent mass, and thus only allow to study the equilibrium shapes of swelling plates [25]. Transient swelling processes are fundamental, for instance, in the toughening of homogeneous [26] and composite gels [27,28].

Motivated by the observations above, here we introduce a large-strain plate theory for polymer gels obtained by consistent dimensional reduction of the three-dimensional, coupled elasticity-solvent migration model established in Ref. [8]. Our theory is not restricted to static equilibrium shapes, but it is also suitable for the study of approach to equilibrium and transient

\* Corresponding author.

E-mail address: [alucanto@sissa.it](mailto:alucanto@sissa.it) (A. Lucantonio).

phenomena. This work extends the recent results presented in Ref. [29], where a membrane theory for swelling polymer gels has been introduced. Our deductive strategy of dimensional reduction employs the weak formulation of the three-dimensional governing equations as a tool to derive the local balance laws for the plate, including the balance of forces, moments and solvent mass. The same deductive approach is employed to obtain the dimensionally reduced counterpart of the three-dimensional swelling constraint, which relates the solvent volume fraction to the volume change of the plate. Thermodynamical consistency is guaranteed through the dissipation inequality, which provides the appropriate constitutive equations for the plate theory, upon introducing for the state variables the same representations along the thickness as those used for the virtual fields. We specialize the constitutive equations for polymer gel plates by employing the Flory-Rehner free energy. In the last section, we study three numerical benchmarks to validate the present plate theory with respect to the parent three-dimensional model. In particular, we show how the proposed plate model can be employed as a computational tool for the shape programming of composite gel plates.

2. Geometry and kinematics of the plate

The ambient space of our theory is represented by the three-dimensional Euclidean point space  $\mathcal{E}$ , whose associated space of translations is denoted by  $\mathcal{V}$ . Unless otherwise stated, free Latin indices range over  $\{0,1,2\}$ , free Greek indices range over  $\{1,2\}$ , and the standard summation convention over repeated indices is employed. Explicit dependence on time of the fields of interest is omitted.

In its reference configuration, the plate occupies a cylindrical region  $\mathcal{B}$  of height  $h$  and mid-surface  $\mathcal{S}$ . For convenience in later computations we parametrize the mid-surface through a generic coordinate system  $(s^1, s^2)$  ranging in a domain  $\mathcal{M} \subset \mathbb{R}^2$ . Denoting by  $\hat{r}(s)$  the point on  $\mathcal{S}$  identified by the coordinates  $s=(s^1, s^2)$  and letting  $\hat{\mathbf{n}}$  denote the unit vector orthogonal to  $\mathcal{S}$ , we can write the typical point of the plate as

$$\hat{\mathbf{z}}(s, \zeta) = \hat{r}(s) + \zeta \hat{\mathbf{n}}, \tag{1}$$

with  $\zeta$  ranging in the interval  $(-h/2, +h/2)$ . We assume that the function  $\hat{r} : \mathcal{M} \rightarrow \mathcal{S}$  is smooth enough so that the forthcoming differential operations performed on  $\hat{r}$  make sense.

Expression (1) provides a parametrization in terms of coordinates  $(s^1, s^2, \zeta)$  for the reference configuration  $\mathcal{B}$  of the plate. The spatial dependence of a (scalar, vectorial, or tensorial) field  $f$  defined on  $\mathcal{B}$  is expressed using this coordinate system, and we write  $f_{,\alpha} = \frac{\partial f}{\partial s^\alpha}$  and  $f_{,3} = \frac{\partial f}{\partial \zeta}$ . In particular, we denote by

$$\hat{\mathbf{g}}_\alpha = \hat{\mathbf{z}}_{,\alpha} = \hat{r}_{,\alpha}, \hat{\mathbf{g}}_3 = \hat{\mathbf{z}}_{,3} = \hat{\mathbf{n}}$$

the referential covariant basis.

With this notation, we can write the area element of the reference base surface as  $da = \hat{\Gamma} ds^1 ds^2$ , with  $\hat{\Gamma} = \hat{\mathbf{g}}_1 \times \hat{\mathbf{g}}_2 \cdot \hat{\mathbf{n}}$ . Moreover, we denote by  $\nu(s)$  the outward unit normal to  $\partial\mathcal{S}$  at  $\hat{\mathbf{z}}(s)$ , and by  $\ell$  the arc-length parameter of  $\partial\mathcal{S}$ . Calculus in curvilinear coordinates yields the formulas

$$\nabla f = \nabla_s f + f_{,3} \otimes \hat{\mathbf{n}}, \quad \nabla_s f = f_{,\alpha} \otimes \hat{\mathbf{g}}^\alpha, \tag{2}$$

(here, the tensor product between a scalar and a vector is the standard multiplication) where the formulas

$$\hat{\mathbf{g}}^1 = \hat{\Gamma}^{-1} \hat{\mathbf{g}}_2 \times \hat{\mathbf{n}}, \quad \hat{\mathbf{g}}^2 = \hat{\Gamma}^{-1} \hat{\mathbf{n}} \times \hat{\mathbf{g}}_1, \quad \hat{\mathbf{g}}^3 = \hat{\mathbf{n}}. \tag{3}$$

express the standard contravariant basis.

The configuration of the plate is described, at each time, by the pair of fields  $(z(s, \zeta), c(s, \zeta))$ , where  $z(s, \zeta)$  is the deformation of the plate and  $c(s, \zeta)$  is the solvent concentration per unit reference volume. Plate theories are usually generated by approximating  $z(s, \zeta)$  with an expression involving a finite number of fields that depend on  $s$  only. The theory we propose in this paper approximates  $z(s, \zeta)$  with the expression

$$z(s, \zeta) = r(s) + \zeta \left( 1 + \frac{\delta(s)}{2} \zeta \right) \mathbf{d}(s) \tag{4}$$

involving three fields: the placement of the mid-surface  $r : \mathcal{M} \rightarrow \mathcal{E}$ , the director  $\mathbf{d} : \mathcal{M} \rightarrow \mathcal{V}$ , and the scalar corrector field  $\delta : \mathcal{M} \rightarrow \mathbb{R}$ . In what follows, we denote by  $\mathbf{a}_\alpha = r_{,\alpha}$  the covariant basis of the tangent plane to the current configuration of the mid-surface. According to (4) the deformation gradient can be expressed as

$$\mathbf{F} = \nabla z = \mathbf{g}_\alpha \otimes \hat{\mathbf{g}}^\alpha + \mathbf{g}_3 \otimes \hat{\mathbf{n}}, \tag{5}$$

where

$$\mathbf{g}_\alpha = \mathbf{a}_\alpha + \zeta \left( 1 + \frac{\delta}{2} \zeta \right) \mathbf{d}_{,\alpha} + \zeta^2 \frac{\delta_{,\alpha}}{2} \mathbf{d}, \quad \mathbf{g}_3 = (1 + \zeta \delta) \mathbf{d}, \tag{6}$$

is the current covariant basis. The vector  $\mathbf{g}_3(s, \zeta)$  represents the image under the deformation  $z(s, \zeta)$  of an infinitesimal material fiber initially placed at  $\hat{\mathbf{z}}(s, \zeta)$  and parallel to  $\hat{\mathbf{n}}$ . As is apparent from (6) the fiber becomes parallel to  $\mathbf{d}$  and undergoes a non-uniform stretch:

$$\lambda_3(s, \zeta) = \sqrt{\hat{\mathbf{F}} \hat{\mathbf{n}} \cdot \hat{\mathbf{F}} \hat{\mathbf{n}}} = \sqrt{\mathbf{g}_3(s, \zeta) \cdot \mathbf{g}_3(s, \zeta)} = |(1 + \delta(s)\zeta) \mathbf{d}(s)|, \tag{7}$$

which does not vanish within the interval  $[-h/2, h/2]$  provided that  $|\delta(s)| < 2/h$ . The introduction of the scalar field  $\delta$  in the kinematics of the plate results into a 7-parameter (the other six parameters are the three components of the displacement  $\mathbf{u}(s) = r(s) - \hat{r}(s)$  of the base surface and the three components of the deformed director  $\mathbf{d}(s)$ ) theory that has been shown to be effective in avoiding locking problems [1] in compressible materials, without performing any manipulation of the three-dimensional constitutive equations before dimensional reduction. Typically, in models using a plane-strain (constant thickness) kinematics, locking is avoided by enforcing the plane-stress hypothesis at the three-dimensional level, which is not compatible with plane-strain, but leads nevertheless to a theory that provides accurate results in many cases.

For the sake of calculation, we shall oftentimes find it is convenient to rewrite the deformation as

$$z(s, \zeta) = r(s) + \zeta \mathbf{d}_1(s) + \frac{\zeta^2}{2} \mathbf{d}_2(s), \quad \mathbf{d}_1 \equiv \mathbf{d}, \quad \mathbf{d}_2 \equiv \delta \mathbf{d}. \tag{8}$$

Then, letting  $\hat{\mathbf{F}} = \nabla_s r = \mathbf{a}_\alpha \otimes \hat{\mathbf{g}}^\alpha$ , we can rewrite (5) as

$$\mathbf{F} = \hat{\mathbf{F}} + \zeta \nabla_s \mathbf{d}_1 + \frac{\zeta^2}{2} \nabla_s \mathbf{d}_2 + (\mathbf{d}_1 + \zeta \mathbf{d}_2) \otimes \hat{\mathbf{n}}. \tag{9}$$

As we will see in Section 5, this two-director representation of  $\mathbf{F}$  is particularly suitable to express the reduced constitutive equations.

Further, we take the concentration  $c$  to be linearly dependent on the thickness coordinate:

$$c(s, \zeta) = c_0(s) + \zeta c_1(s). \tag{10}$$

Importantly, we observe that, in principle, neither (4) nor (10) are

necessary for the determination of the balance equations of the plate theory from the principle of virtual power, since for that aim only the representations of the virtual fields are involved. Thus, the use of (4), (10) is effectively restricted to performing explicit integrations along the thickness in the derivation of reduced constitutive equations (see Section 5).

### 3. Balance equations

#### 3.1. Balance of forces and moments

Following [30,31], we derive the balance of forces and moments for the plate-like body  $\mathcal{B}$  starting from the principle of virtual power

$$\mathcal{A}_m^h(\mathcal{M}, \tilde{\mathbf{v}}) = \mathcal{W}_m^h(\mathcal{M}, \tilde{\mathbf{v}}), \tag{11}$$

which states the equality between the virtual expenditures of internal mechanical power

$$\mathcal{A}_m^h(\mathcal{M}, \tilde{\mathbf{v}}) = \int_{\mathcal{M}} \int_{-h/2}^{h/2} \mathbf{S} \cdot \nabla \tilde{\mathbf{v}} \, d\zeta da \tag{12}$$

and external mechanical power

$$\begin{aligned} \mathcal{W}_m^h(\mathcal{M}, \tilde{\mathbf{v}}) &= \int_{\mathcal{M}} \int_{-h/2}^{h/2} \mathbf{f} \cdot \tilde{\mathbf{v}} \, d\zeta da + \int_{\mathcal{M}} (\mathbf{t} \cdot \tilde{\mathbf{v}})|_{\pm h/2} da \\ &+ \int_{\partial \mathcal{M}} \int_{-h/2}^{h/2} \mathbf{t} \cdot \tilde{\mathbf{v}} \, d\zeta dl, \end{aligned} \tag{13}$$

for any virtual velocity field  $\tilde{\mathbf{v}}$ . Here,  $\mathbf{S}$  is the Piola-Kirchhoff stress and the system of external forces is represented by the body force  $\mathbf{f}$  acting on  $\mathcal{B}$  and the surface traction  $\mathbf{t}$  acting on  $\partial \mathcal{B}$ . The crucial point when using (11) is to restrict test velocities to those compatible with the kinematic constraint that generates the theory. Here, consistent with the expression (8) of the deformation of the plate, we assume that, for  $s$  fixed, the virtual velocity field is a quadratic polynomial of  $\zeta$ :

$$\tilde{\mathbf{v}}(s, \zeta) = \tilde{\mathbf{v}}_0(s) + \zeta \tilde{\mathbf{v}}_1(s) + \frac{\zeta^2}{2} \tilde{\mathbf{v}}_2(s), \tag{14}$$

so that the internal virtual power expended is

$$\begin{aligned} \int_{\mathcal{M}} \int_{-h/2}^{h/2} \left[ \mathbf{S} \cdot \left( \nabla_s \tilde{\mathbf{v}}_0 + \zeta \nabla_s \tilde{\mathbf{v}}_1 + \frac{\zeta^2}{2} \nabla_s \tilde{\mathbf{v}}_2 \right) \right] d\zeta da \\ + \int_{\mathcal{M}} \int_{-h/2}^{h/2} [\mathbf{s} \cdot (\tilde{\mathbf{v}}_1 + \zeta \tilde{\mathbf{v}}_2)] d\zeta da, \end{aligned} \tag{15}$$

where  $\mathbf{S} = \mathbf{S}\hat{\mathbf{P}}$ ,  $\mathbf{s} = \mathbf{S}\hat{\mathbf{n}}$  with  $\hat{\mathbf{P}} = \hat{\mathbf{g}}_\alpha \otimes \hat{\mathbf{g}}^\alpha$  the in-plane projector. Introducing the stress resultants<sup>1</sup>

<sup>1</sup> Following standard convention we set  $0! = 1$ . As a rule, given a field  $\varphi(s, \zeta)$  we let  $\varphi^{(i)}(s) = \int_{-h/2}^{h/2} \frac{\zeta^i}{i!} \varphi(s, \zeta) d\zeta$  denote its moment of order  $i$  with respect to the variable  $\zeta$ .

$$\mathbf{S}^{(i)}(s) = \int_{-h/2}^{h/2} \frac{\zeta^i}{i!} \mathbf{S}(s, \zeta) d\zeta, \tag{16a}$$

$$\mathbf{s}^{(i)}(s) = \int_{-h/2}^{h/2} \frac{\zeta^i}{i!} \mathbf{s}(s, \zeta) d\zeta, \tag{16b}$$

we can recast (15) as

$$\mathcal{A}_m(\mathcal{M}, \tilde{\mathbf{v}}_i) = \int_{\mathcal{M}} \left( \mathbf{S}^{(i)} \cdot \nabla_s \tilde{\mathbf{v}}_i + \mathbf{s}^{(0)} \cdot \tilde{\mathbf{v}}_1 + \mathbf{s}^{(1)} \cdot \tilde{\mathbf{v}}_2 \right) da. \tag{17}$$

Likewise, introducing the bulk force resultants

$$\mathbf{f}^{(i)}(s) = \int_{-h/2}^{h/2} \frac{\zeta^i}{i!} \mathbf{f}(s, \zeta) d\zeta + \left( \frac{\zeta^i}{i!} \mathbf{t}(s, \zeta) \right)_{\zeta=-h/2} + \left( \frac{\zeta^i}{i!} \mathbf{t}(s, \zeta) \right)_{\zeta=h/2} \tag{18}$$

defined for  $s \in \mathcal{M}$ , and the boundary force resultants

$$\mathbf{t}^{(i)}(s) = \int_{-h/2}^{h/2} \frac{\zeta^i}{i!} \mathbf{t}(s, \zeta) d\zeta \tag{19}$$

defined for  $s \in \partial \mathcal{M}$ , we can write the external power as

$$\mathcal{W}_m(\mathcal{M}, \tilde{\mathbf{v}}_i) = \int_{\mathcal{M}} \left( \mathbf{f}^{(i)} \cdot \tilde{\mathbf{v}}_i \right) da + \int_{\partial \mathcal{M}} \left( \mathbf{t}^{(i)} \cdot \tilde{\mathbf{v}}_i \right) dl. \tag{20}$$

When deriving balance equations in strong form by exploiting the arbitrariness of the virtual fields, some care is required, because the virtual velocities  $\tilde{\mathbf{v}}_1$  and  $\tilde{\mathbf{v}}_2$  are not independent. Indeed, it holds  $\tilde{\mathbf{v}}_2 = \delta \mathbf{d} + \delta \tilde{\mathbf{v}}_1$ , since  $\mathbf{d}_2 = \delta \mathbf{d}$ . Substitution of this relation into the virtual-power functionals (17) and (20), yields, for the internal power

$$\mathcal{A}'_m(\mathcal{M}, \tilde{\mathbf{v}}_0, \tilde{\mathbf{v}}_1, \tilde{\delta}) = \int_{\mathcal{M}} \left( \mathbf{N} \cdot \nabla_s \tilde{\mathbf{v}}_0 + \mathbf{M} \cdot \nabla_s \tilde{\mathbf{v}}_1 + \mathbf{q} \cdot \tilde{\mathbf{v}}_1 + \boldsymbol{\tau} \cdot \nabla_s \tilde{\delta} + \tau \tilde{\delta} \right) da, \tag{21}$$

where

$$\begin{aligned} \mathbf{N} &= \mathbf{S}^{(0)}, \quad \mathbf{M} = \mathbf{S}^{(1)} + \delta \mathbf{S}^{(2)}, \\ \mathbf{q} &= \mathbf{s}^{(0)} + \delta \mathbf{s}^{(1)} + \mathbf{S}^{(2)} \nabla_s \delta, \\ \boldsymbol{\tau} &= \mathbf{S}^{(2)\top} \mathbf{d}, \quad \tau = \mathbf{s}^{(1)} \cdot \mathbf{d} + \mathbf{S}^{(2)} \cdot \nabla_s \mathbf{d}, \end{aligned} \tag{22}$$

and, for the external power

$$\begin{aligned} \mathcal{W}'_m(\mathcal{M}, \tilde{\mathbf{v}}_0, \tilde{\mathbf{v}}_1, \tilde{\delta}) &= \int_{\mathcal{M}} \left( \mathbf{f}^{(0)} \cdot \tilde{\mathbf{v}}_0 + \bar{\mathbf{f}}^{(1)} \cdot \tilde{\mathbf{v}}_1 + f_d^{(2)} \tilde{\delta} \right) da \\ &+ \int_{\partial \mathcal{M}} \left( \mathbf{t}^{(0)} \cdot \tilde{\mathbf{v}}_0 + \bar{\mathbf{t}}^{(1)} \cdot \tilde{\mathbf{v}}_1 + t_d^{(2)} \tilde{\delta} \right) dl, \end{aligned} \tag{23}$$

where

$$\begin{aligned} \bar{\mathbf{f}}^{(1)} &= \mathbf{f}^{(1)} + \delta \mathbf{f}^{(2)}, \quad f_d^{(2)} = \mathbf{f}^{(2)} \cdot \mathbf{d}, \\ \bar{\mathbf{t}}^{(1)} &= \mathbf{t}^{(1)} + \delta \mathbf{t}^{(2)}, \quad t_d^{(2)} = \mathbf{t}^{(2)} \cdot \mathbf{d}. \end{aligned} \tag{24}$$

For simplicity, we assume that the boundary  $\partial \mathcal{M}$  is partitioned into

disjoint parts  $\partial_m^0 \mathcal{M}$  and  $\partial_m^1 \mathcal{M}$ , with natural (essential) boundary conditions being prescribed on the former (latter). Then, from the arbitrariness of  $(\tilde{\mathbf{v}}_0, \tilde{\mathbf{v}}_1, \tilde{\delta})$  in the virtual–power balance

$$\mathcal{G}'_m(\mathcal{M}, \tilde{\mathbf{v}}_0, \tilde{\mathbf{v}}_1, \tilde{\delta}) = \mathcal{W}'_c(\mathcal{M}, \tilde{\mathbf{v}}_0, \tilde{\mathbf{v}}_1, \tilde{\delta}) \quad (25)$$

we deduce the balance equations and the corresponding natural boundary conditions, namely,

$$\text{div}_s \mathbf{N} + \mathbf{f}^{(0)} = 0, \quad \text{in } \mathcal{M}, \quad (26a)$$

$$\text{div}_s \mathbf{M} - \mathbf{q} + \bar{\mathbf{f}}^{(1)} = 0, \quad \text{in } \mathcal{M}, \quad (26b)$$

$$\text{div}_s \boldsymbol{\tau} - \boldsymbol{\tau} + \mathbf{f}_d^{(2)} = 0, \quad \text{in } \mathcal{M}, \quad (26c)$$

and

$$\mathbf{N}\boldsymbol{\nu} = \mathbf{t}^{(0)}, \quad \text{on } \partial_m^0 \mathcal{M}, \quad (27a)$$

$$\mathbf{M}\boldsymbol{\nu} = \bar{\mathbf{t}}^{(1)}, \quad \text{on } \partial_m^0 \mathcal{M}, \quad (27b)$$

$$\boldsymbol{\tau} \cdot \boldsymbol{\nu} = \mathbf{t}_d^{(2)}, \quad \text{on } \partial_m^0 \mathcal{M}. \quad (27c)$$

It is easily checked that the symmetry condition  $\mathbf{S}\mathbf{F}^T \in \text{Sym}$  entails

$$\mathbf{N}\hat{\mathbf{F}}^T + \mathbf{M}\nabla_s \mathbf{d}^T + \mathbf{q} \otimes \mathbf{d} \in \text{Sym}. \quad (28)$$

The tensorial identity (28) is equivalent to

$$\mathbf{n}^\alpha \times \mathbf{a}_\alpha + \mathbf{m}^\alpha \times \mathbf{d}_{,\alpha} + \mathbf{q} \times \mathbf{d} = 0, \quad (29)$$

where  $\mathbf{n}^\alpha = \mathbf{N}\hat{\mathbf{g}}^\alpha$  and  $\mathbf{m}^\alpha = \mathbf{M}\hat{\mathbf{g}}^\alpha$ . This relation can also be obtained by imposing invariance of the internal power expended within every part of the plate under superposed rigid velocity fields. In view of (29), by taking the cross and scalar products of (26b) with  $\mathbf{d}$  we obtain, respectively,

$$\text{div}_s(\mathbf{D}\mathbf{M}) - \mathbf{n}^\alpha \times \mathbf{a}_\alpha + \mathbf{d} \times \bar{\mathbf{f}}^{(1)} = 0, \quad (30a)$$

$$\text{div}_s(\mathbf{M}^T \mathbf{d}) - \mathbf{M} \cdot \nabla_s \mathbf{d} - \mathbf{d} \cdot \mathbf{q} + \mathbf{d} \cdot \bar{\mathbf{f}}^{(1)} = 0, \quad (30b)$$

where  $\mathbf{D}$  is the skew tensor associated to  $\mathbf{d}$ . From (30), we can recover the classical forms of the balances of torques and director forces for a 6-parameter plate by setting  $\tilde{\delta} = 0$ , see Refs. [30,31]. For a 7-parameter plate, these equations are supplemented by the second-order balance of director forces (26c).

### 3.2. Balance of solvent mass

In the applications consider here, a flux of solvent is prescribed over the lateral surface of the plate, including the top and bottom faces. The strong form of the balance of solvent mass reads

$$\dot{c} + \text{div } \mathbf{h} = 0, \quad \text{in } \mathcal{B}, \quad (31a)$$

$$-\mathbf{h} \cdot \boldsymbol{\nu} = \beta, \quad \text{on } \partial \mathcal{M} \times (-h/2, +h/2), \quad (31b)$$

where  $\mathbf{h}$  is the referential solvent flux, and  $\beta$  is a surface supply of solvent.

With a view towards obtaining a reduced theory, we replace the pointwise statements (31) with their weak form. Inspired by Ref. [32], we interpret such weak form as a version of the

virtual-power principle whereby chemical potential is a test field that enters along with its gradient in the power expenditure. Specifically, we prescribe the following representations for virtual expenditures of internal chemical power

$$\mathcal{G}_c^h(\mathcal{M}, \tilde{\mu}) = \int_{\mathcal{M}} \int_{-h/2}^{h/2} (\dot{c}\tilde{\mu} - \mathbf{h} \cdot \nabla \tilde{\mu}) d\zeta da, \quad (32)$$

and external chemical power

$$\mathcal{W}_c^h(\mathcal{M}, \tilde{\mu}) = \int_{\partial \mathcal{M}} \int_{-h/2}^{h/2} \beta \tilde{\mu} d\zeta d\ell + \int_{\mathcal{M} \times \left\{ \begin{smallmatrix} +\frac{h}{2} \\ -\frac{h}{2} \end{smallmatrix} \right\}} \beta \tilde{\mu} da. \quad (33)$$

Then, the three-dimensional pointwise balance equation (31) are recovered on imposing that the external and internal chemical powers be balanced

$$\mathcal{G}_c^h(\mathcal{M}, \tilde{\mu}) = \mathcal{W}_c^h(\mathcal{M}, \tilde{\mu}) \quad (34)$$

for any virtual chemical potential  $\tilde{\mu}$ .

To arrive at a system of reduced equations, we enforce the principle of virtual power (34) on the class of virtual chemical potentials that depend linearly on  $\zeta$ :

$$\tilde{\mu}(s, \zeta) = \tilde{\mu}_0(s) + \zeta \tilde{\mu}_1(s), \quad (35)$$

consistent with the representation (10) for the work-conjugate field  $c$ . Granted (35) and using (2) with  $f = \tilde{\mu}$ , we can write the internal chemical power as:

$$\mathcal{G}_c(\mathcal{M}, \tilde{\mu}_0, \tilde{\mu}_1) = \int_{\mathcal{M}} \left( \dot{c}^{(0)} \tilde{\mu}_0 + \dot{c}^{(1)} \tilde{\mu}_1 - \mathbf{h}^{(0)} \cdot \nabla_s \tilde{\mu}_0 - h_3^{(0)} \tilde{\mu}_1 - \mathbf{h}^{(1)} \cdot \nabla_s \tilde{\mu}_1 \right) da, \quad (36)$$

where we have introduced the moments of the concentration

$$c^{(i)}(s) = \int_{-h/2}^{h/2} \frac{\zeta^i}{i!} c(s, \zeta) d\zeta, \quad (37)$$

and of the solvent flux

$$\mathbf{h}^{(i)}(s) = \int_{-h/2}^{h/2} \frac{\zeta^i}{i!} \mathbf{h}(s, \zeta) d\zeta, \quad \mathbf{h} = \dot{\mathbf{P}}\mathbf{h}, \quad (38a)$$

$$h_3^{(i)}(s) = \int_{-h/2}^{h/2} \frac{\zeta^i}{i!} h_3(s, \zeta) d\zeta, \quad h_3 = \mathbf{h} \cdot \hat{\mathbf{n}}. \quad (38b)$$

Likewise, the external power becomes

$$\mathcal{W}_c(\mathcal{M}, \tilde{\mu}_0, \tilde{\mu}_1) = \int_{\partial \mathcal{M}} \left( \beta^{(0)} \tilde{\mu}_0 + \beta^{(1)} \tilde{\mu}_1 \right) d\ell + \int_{\mathcal{M}} \left( \bar{\beta}^{(0)} \tilde{\mu}_0 + \bar{\beta}^{(1)} \tilde{\mu}_1 \right) da, \quad (39)$$

where

$$\beta^{(i)}(s) = \int_{-h/2}^{h/2} \frac{\zeta^i}{i!} \beta(s, \zeta) d\zeta, \quad s \in \partial \mathcal{M}, \quad (40a)$$

$$\bar{\beta}^{(i)}(s) = \sum_{\zeta=\pm h/2} \frac{\zeta^i}{i!} \beta(s, \zeta) d\zeta, \quad s \in \mathcal{M}. \quad (40b)$$

With these definitions the principle of virtual power (34) may be written as

$$\mathcal{A}_c(\mathcal{M}, \tilde{\mu}_0, \tilde{\mu}_1) = \mathcal{W}_c(\mathcal{M}, \tilde{\mu}_0, \tilde{\mu}_1) \quad (41)$$

for any  $\tilde{\mu}_0$  and  $\tilde{\mu}_1$ .

We partition the boundary of  $\mathcal{M}$  into parts  $\partial_c^0 \mathcal{M}$  and  $\partial_c^1 \mathcal{M}$ , and we impose essential boundary conditions for the chemical potential on  $\partial_c^1 \mathcal{M}$ . On exploiting the arbitrariness of the virtual chemical potential, i.e. of the fields  $\tilde{\mu}_0$  and  $\tilde{\mu}_1$ , in  $\mathcal{M} \cup \partial_c^0 \mathcal{M}$ , we obtain the balance equations

$$\dot{c}^{(0)} + \text{div}_s \mathbf{h}^{(0)} = \bar{\beta}^{(0)}, \quad \text{in } \mathcal{M}, \quad (42a)$$

$$\dot{c}^{(1)} + \text{div}_s \mathbf{h}^{(1)} - h_3^{(0)} = \bar{\beta}^{(1)}, \quad \text{in } \mathcal{M}, \quad (42b)$$

and the natural boundary conditions

$$-\mathbf{h}^{(0)} \cdot \mathbf{v} = \beta^{(0)}, \quad \text{on } \partial_c^0 \mathcal{M}, \quad (43a)$$

$$-\mathbf{h}^{(1)} \cdot \mathbf{v} = \beta^{(1)}, \quad \text{on } \partial_c^0 \mathcal{M}. \quad (43b)$$

Notice that the above equations do not give explicitly the concentration field. However, if we assume that the concentration field has the representation (10), then we can obtain from (42) a set of evolution equations for  $c_0$  and  $c_1$ . To this aim, it suffices to make use of the following identities:

$$c^{(0)} = hc_0, \quad c^{(1)} = \frac{h^3}{12} c_1. \quad (44a)$$

Then, the balance equation (42) become

$$h\dot{c}_0 + \text{div}_s \mathbf{h}^{(0)} = \bar{\beta}^{(0)}, \quad \text{in } \mathcal{M}, \quad (45a)$$

$$\frac{h^3}{12} \dot{c}_1 + \text{div}_s \mathbf{h}^{(1)} - h_3^{(0)} = \bar{\beta}^{(1)}, \quad \text{in } \mathcal{M}. \quad (45b)$$

**Remark: essential boundary conditions for chemical potential.** In the considerations leading to (45), essential boundary conditions for chemical potential have been imposed only on the lateral mantle  $\partial \mathcal{M} \times \left(-\frac{h}{2}, \frac{h}{2}\right)$  of the plate. This restriction can be easily removed, and one can impose essential conditions on parts of the top and bottom face of the plate, to be handled by making use of Lagrange multipliers. To be specific: let the boundary values of the chemical potential field be assigned values  $\mu^-$  and  $\mu^+$  on parts of the top and bottom faces, which we denote by  $\mathcal{M}^+ \times \left\{\frac{h}{2}\right\}$  and  $\mathcal{M}^- \times \left\{\frac{h}{2}\right\}$ , with  $\mathcal{M}^+ \subseteq \mathcal{M}$  and  $\mathcal{M}^- \subseteq \mathcal{M}$ . Then, denoting by  $\chi^+ : \mathcal{M} \rightarrow \{0, 1\}$  and  $\chi^- : \mathcal{M} \rightarrow \{0, 1\}$  the characteristic functions of  $\mathcal{M}^+$  and  $\mathcal{M}^-$ , respectively, we add the following reactive term

$$\mathcal{W}_c^r(\mathcal{M}, \tilde{\mu}_0, \tilde{\mu}_1) = \int_{\mathcal{M}} \left( \chi^+ r^+ \left( \tilde{\mu}_0 + \frac{h}{2} \tilde{\mu}_1 \right) + \chi^- r^- \left( \tilde{\mu}_0 + \frac{h}{2} \tilde{\mu}_1 \right) \right) da$$

to the external power (39). Then, the additional reactive contributions  $\chi^+ r^+$  and  $\chi^- r^-$  and  $\frac{h}{2}(\chi^+ r^+ - \chi^- r^-)$  appear on the right-hand sides of the first and second equation in (45), respectively.

#### 4. Swelling constraint

For a poroelastic medium undergoing large strain, the assumption of incompressibility of both the solid and the solvent implies that the deformation gradient  $\mathbf{F}$  and the concentration  $c$  obey the *incompressibility constraint* [6,8]

$$J = \det \mathbf{F} = 1 + \Omega(c - c_\star), \quad (46)$$

where  $c_\star$  is the homogeneous solvent concentration in the reference state. Since the deformation is a polynomial of degree 2 with respect to  $\zeta$ , its determinant is a polynomial of degree 6 with respect to the same variable. Now, recalling from (10) that concentration is a first-order polynomial in  $\zeta$ , the constraint (46) cannot be satisfied pointwise.

This state of matters leads us to *relax* constraint (46), by replacing it with a weak constraint

$$\int_{\mathcal{M}} \int_{-h/2}^{h/2} \gamma [1 - \Omega(c - c_\star)] \bar{p} d\zeta da = 0, \quad (47)$$

where the *virtual pressure*  $\bar{p}$  has the representation  $\bar{p}(s, \zeta) = \bar{p}_0(s) + \zeta \bar{p}_1(s)$ . By enforcing the weak form of the incompressibility constraint with degree-1 virtual pressures we are going to deduce, for each point  $s$  of the base surface, a set of two equations relating the deformation with the fields  $c_0$  and  $c_1$ .

From the identity  $J = (\mathbf{F}\hat{\mathbf{g}}_1 \times \mathbf{F}\hat{\mathbf{g}}_2 \cdot \mathbf{F}\hat{\mathbf{n}}) / (\hat{\mathbf{g}}_1 \times \hat{\mathbf{g}}_2 \cdot \hat{\mathbf{n}})$  and from (5) we find  $J = \mathbf{g}_1 \times \mathbf{g}_2 \cdot \mathbf{g}_3 / \hat{\Gamma}$ . Thus, using (6) we compute:

$$J = \left( \mathbf{r}_0 + \zeta \mathbf{r}_1 + \frac{\zeta^2}{2} \mathbf{r}_2 \right) \cdot (1 + \zeta \delta) \mathbf{d} + o(\zeta^2), \quad (48)$$

with

$$\begin{aligned} \mathbf{r}_0 &= \frac{\mathbf{a}_1 \times \mathbf{a}_2}{\hat{\Gamma}}, \quad \mathbf{r}_1 = \frac{\mathbf{d}_{,1} \times \mathbf{a}_2 - \mathbf{d}_{,2} \times \mathbf{a}_1}{\hat{\Gamma}}, \\ \mathbf{r}_2 &= \delta \mathbf{r}_1 + \frac{(\delta_{,2} \mathbf{a}_1 - \delta_{,1} \mathbf{a}_2) \times \mathbf{d} + 2\mathbf{d}_{,1} \times \mathbf{d}_{,2}}{\hat{\Gamma}}. \end{aligned} \quad (49)$$

Then, we rely on the arbitrariness of  $\bar{p}_0(s)$  and  $\bar{p}_1(s)$  to obtain the pair of equations holding pointwise in  $\mathcal{M}$ :

$$1 + \Omega(c_0 - c_\star) = \mathbf{r}_0 \cdot \mathbf{d} + \frac{h^2}{24} (2\delta \mathbf{r}_1 + \mathbf{r}_2) \cdot \mathbf{d}, \quad (50a)$$

$$\Omega c_1 = (\delta \mathbf{r}_0 + \mathbf{r}_1) \cdot \mathbf{d}. \quad (50b)$$

#### 5. Thermodynamics and constitutive equations

In this section we obtain constitutive equations for the stress resultants and the flux resultants, starting from those that govern the large-strain behavior of three dimensional poroelastic bodies with incompressible constituents. We first deduce general

reduce height of the brackets

relations; then, we consider the specialization of these relations to composite polymer gel plates.

5.1. General relations

We begin by assuming that the free energy per unit referential volume obeys the constitutive equation

$$\psi = \widehat{\psi}(\mathbf{F}, c). \tag{51}$$

For  $\mathcal{P} \subset \mathcal{M}$  we write the dissipation inequality as

$$\int_{\mathcal{P}} \int_{-h/2}^{h/2} [\dot{\psi} - p(\mathbf{F}^* \cdot \dot{\mathbf{F}} - \Omega \dot{c})] d\zeta da \leq \mathcal{A}_m^h(\mathcal{P}, \mathbf{v}) + \mathcal{A}_c^h(\mathcal{P}, \mu), \tag{52}$$

where  $\mathcal{A}_m^h(\mathcal{P}, \mathbf{v})$  and  $\mathcal{A}_c^h(\mathcal{P}, \mu)$  are, respectively, the mechanical and the chemical powers given in (12) and (32) expended within a part  $\mathcal{P} \times (-h/2, +h/2)$  on the actual velocity  $\mathbf{v} = \dot{\mathbf{z}}$  and chemical potential. Here,  $\mathbf{F}^*$  is the cofactor of  $\mathbf{F}$ :

$$\mathbf{F}^* = \sum_{i=1}^3 J \mathbf{g}^i \otimes \hat{\mathbf{g}}_i, \tag{53}$$

where

$$\mathbf{g}^1 = \frac{\mathbf{g}_2 \times \mathbf{g}_3}{\Gamma}, \quad \mathbf{g}^2 = \frac{\mathbf{g}_3 \times \mathbf{g}_1}{\Gamma}, \quad \mathbf{g}^3 = \frac{\mathbf{g}_1 \times \mathbf{g}_2}{\Gamma}, \tag{54}$$

with  $\Gamma = \mathbf{g}_1 \times \mathbf{g}_2 \cdot \mathbf{g}_3$

are the contravariant basis vectors in the current configuration.

We consider evolution processes such that the deformation and the concentration obey the restrictions (4) and (10). For any such process, the velocity and the swelling rate (the time derivative of the concentration) have the form

$$\mathbf{v}(s, \zeta) = \mathbf{v}_0(s) + \zeta \mathbf{v}_1(s) + \frac{\zeta^2}{2} \mathbf{v}_2(s), \tag{55a}$$

$$\dot{c}(s, \zeta) = \dot{c}_0(s) + \zeta \dot{c}_1(s). \tag{55b}$$

From (55) and from the constitutive equation (51) we obtain

$$\int_{-h/2}^{h/2} \dot{\psi} d\zeta da = (\partial_{\mathbf{F}} \widehat{\psi})^{(i)} \cdot \nabla_s \mathbf{v}_i + (\partial_{\mathbf{F}} \widehat{\psi})^{(0)} [\dot{\mathbf{n}}] \cdot \mathbf{v}_1 + (\partial_{\mathbf{F}} \widehat{\psi})^{(1)} [\dot{\mathbf{n}}] \cdot \mathbf{v}_2 + (\partial_c \widehat{\psi})^{(0)} \dot{c}_0 + (\partial_c \widehat{\psi})^{(1)} \dot{c}_1, \tag{56}$$

where

$$(\partial_{\mathbf{F}} \widehat{\psi})^{(i)} = \left( \int_{-h/2}^{h/2} \frac{\zeta^i}{i!} \partial_{\mathbf{F}} \widehat{\psi}(\mathbf{F}, c) d\zeta \right) \hat{\mathbf{P}}, \tag{57a}$$

$$(\partial_c \widehat{\psi})^{(i)} = \int_{-h/2}^{h/2} \frac{\zeta^i}{i!} \partial_c \widehat{\psi}(\mathbf{F}, c) d\zeta. \tag{57b}$$

Thanks to the identity (53), we have the following representation for the pressure power:

$$\int_{-h/2}^{h/2} p \mathbf{F}^* \cdot \dot{\mathbf{F}} d\zeta = \mathbf{S}_p^{(i)} \cdot \nabla_s \mathbf{v}_i + \mathbf{s}_p^{(0)} \cdot \mathbf{v}_1 + \mathbf{s}_p^{(1)} \cdot \mathbf{v}_2, \tag{58}$$

where

$$\mathbf{S}_p^{(i)} = \left( \int_{-h/2}^{h/2} \frac{\zeta^i}{i!} p J \mathbf{g}^\alpha d\zeta \right) \otimes \hat{\mathbf{g}}_\alpha, \tag{59a}$$

$$\mathbf{s}_p^{(i)} = \int_{-h/2}^{h/2} \frac{\zeta^i}{i!} p J \mathbf{g}^3 d\zeta. \tag{59b}$$

Finally, consistent with the representation of the virtual chemical potential we have selected in (35) to enforce mass balance, we assume that the chemical potential has the form

$$\mu(s, \zeta) = \mu_0(s) + \zeta \mu_1(s). \tag{60}$$

Then, with calculations analogous to those leading to (17) and (36), the internal powers in (52) may be recast as  $\mathcal{A}_m(\mathcal{P}, \mathbf{v}_i)$  and  $\mathcal{A}_c(\mathcal{P}, \mu_0, \mu_1)$ , respectively, where the virtual fields in (17) and (36) are replaced by the actual fields  $\mathbf{v}_i$  and  $\mu_i$ .

On account of the reduced representations of the internal powers and the expressions (56) and (58) for the time rate of the free energy and the reactive power, the dissipation inequality (52) reads

$$\int_{\mathcal{P}} \left[ \left( (\partial_{\mathbf{F}} \widehat{\psi})^{(i)} + \mathbf{S}_p^{(i)} \right) \cdot \nabla_s \mathbf{v}_i + \left( (\partial_{\mathbf{F}} \widehat{\psi})^{(0)} [\dot{\mathbf{n}}] - \mathbf{s}_p^{(0)} \right) \cdot \mathbf{v}_1 + \left( (\partial_{\mathbf{F}} \widehat{\psi})^{(1)} [\dot{\mathbf{n}}] - \mathbf{s}_p^{(1)} \right) \cdot \mathbf{v}_2 \right] da + \int_{\mathcal{P}} \left[ \left( (\partial_c \widehat{\psi})^{(0)} - p^{(0)} \right) \dot{c}_0 + \left( (\partial_c \widehat{\psi})^{(1)} - p^{(1)} \right) \dot{c}_1 \right] da \leq \int_{\mathcal{P}} \left( \mathbf{S}^{(i)} \cdot \nabla_s \mathbf{v}_i + \mathbf{s}^{(0)} \cdot \mathbf{v}_1 + \mathbf{s}^{(1)} \cdot \mathbf{v}_2 \right) da + \int_{\mathcal{P}} \left( \mu^{(0)} \dot{c}_0 + \mu^{(1)} \dot{c}_1 - \mathbf{h}^{(0)} \cdot \nabla_s \mu_0 - h_3^{(0)} \mu_1 - \mathbf{h}^{(1)} \cdot \nabla_s \mu_1 \right) da, \tag{61}$$

where

$$\mu^{(i)}(s) = \int_{-h/2}^{h/2} \frac{\zeta^i}{i!} \mu(s, \zeta) d\zeta, \tag{62}$$

and

$$p^{(i)}(s) = \int_{-h/2}^{h/2} \frac{\zeta^i}{i!} p(s, \zeta) d\zeta. \tag{63}$$

Consistent with the requirement that (61) holds for every choice of the velocities (55) we prescribe

$$\mathbf{s}^{(i)} = (\partial_{\mathbf{F}} \widehat{\psi})^{(i)} - \mathbf{S}_p^{(i)}, \quad i = 0, 1, 2, \tag{64a}$$

$$\mathbf{s}^{(i)} = (\partial_{\mathbf{F}} \widehat{\psi})^{(i)} \left[ \mathbf{n} \right] - \mathbf{s}_p^{(i)}, \quad i = 0, 1, \tag{64b}$$

$$\boldsymbol{\mu}^{(i)} = (\partial_c \widehat{\psi})^{(i)} + \Omega p^{(i)}, \quad i = 0, 1. \tag{64c}$$

Using (64), we obtain from (61) the following reduced dissipation inequality

$$- \int_{\mathcal{P}} (\mathbf{h}^{(0)} \cdot \nabla_s \mu_0 + h_3^{(0)} \mu_1 + \mathbf{h}^{(1)} \cdot \nabla_s \mu_1) da \geq 0. \tag{65}$$

A selection criterion for the constitutive equations governing the fluxes  $\mathbf{h}^{(0)}$ ,  $\mathbf{h}^{(1)}$  and  $h_3^{(0)}$  can be obtained by requiring consistency with the three-dimensional constitutive law of Darcy type

$$\mathbf{h} = - \frac{cD}{\mathcal{R}T} \nabla \mu, \tag{66}$$

where  $D$  is the solvent diffusivity,  $\mathcal{R}$  is the universal gas constant and  $T$  is the absolute temperature. Integrating along the thickness in accord with the definitions (38), and using the representations (10) and (60), we have

$$\mathbf{h}^{(0)} = - \frac{D}{\mathcal{R}T} h \left( c_0 \nabla_s \mu_0 + \frac{h^2}{12} c_1 \nabla_s \mu_1 \right), \tag{67a}$$

$$\mathbf{h}^{(1)} = - \frac{D}{\mathcal{R}T} \frac{h^3}{12} (c_1 \nabla_s \mu_0 + c_0 \nabla_s \mu_1), \tag{67b}$$

$$h_3^{(0)} = - \frac{c_0 D}{\mathcal{R}T} h \mu_1. \tag{67c}$$

In view of (64c), and consistent with representation (60) of the chemical potential, we write the pressure as a linear function of  $\zeta$ :

$$p(s, \zeta) = p_0(s) + \zeta p_1(s). \tag{68}$$

With this and the definitions (49), the reactive stress resultants (59) can be rendered explicitly as

$$\mathbf{S}_p^{(0)} = h \left( p_0 + p_1 \frac{h^2}{12} \delta \right) \mathbf{R}_0 + \frac{h^3}{12} \left( p_1 + p_0 \frac{3}{2} \delta \right) \mathbf{R}_1, \tag{69a}$$

$$\mathbf{S}_p^{(1)} = \frac{h^3}{12} (\delta p_0 + p_1) \mathbf{R}_0 + \frac{h^3}{12} p_1 \mathbf{R}_1, \tag{69b}$$

$$\mathbf{S}_p^{(2)} = \frac{h^3}{12} p_0 \mathbf{R}_0, \tag{69c}$$

$$\mathbf{s}_p^{(0)} = h p_0 \left( \mathbf{r}_0 + \frac{h^2}{24} \mathbf{r}_2 \right) + \frac{h^3}{12} p_1 \mathbf{r}_1, \tag{69d}$$

$$\mathbf{s}_p^{(1)} = \frac{h^3}{12} (p_0 \mathbf{r}_1 + p_1 \mathbf{r}_0), \tag{69e}$$

where

$$\mathbf{R}_0 = \frac{1}{\Gamma} \left[ (\mathbf{a}_2 \times \mathbf{d}) \otimes \mathbf{g}_1 - (\mathbf{a}_1 \times \mathbf{d}) \otimes \mathbf{g}_2 \right], \tag{70a}$$

$$\mathbf{R}_1 = \frac{1}{\Gamma} \left[ (\mathbf{d}_{,2} \times \mathbf{d}) \otimes \mathbf{g}_1 - (\mathbf{d}_{,1} \times \mathbf{d}) \otimes \mathbf{g}_2 \right], \tag{70b}$$

where we have to retained terms up to  $O(h^3)$ . Then, recalling (68), we deduce the following relations from (64c):

$$\boldsymbol{\mu}^{(0)} = (\partial_c \widehat{\psi})^{(0)} + \Omega h p_0, \tag{71a}$$

$$\boldsymbol{\mu}^{(1)} = (\partial_c \widehat{\psi})^{(1)} + \Omega \frac{h^3}{12} p_1. \tag{71b}$$

A handier constitutive equation can be obtained by recalling that  $c(s, \zeta) = c_0(s) + \zeta c_1(s)$  and the Taylor expansion

$$\partial_c \widehat{\psi}(\mathbf{F}, c_0) = \partial_c \widehat{\psi}(\mathbf{F}, c_0) + \partial_c^2 \widehat{\psi}(\mathbf{F}, c_0) \zeta c_1 + \frac{\partial_c^3 \widehat{\psi}(\mathbf{F}, c_0)}{2} \zeta^2 c_1^2 + o(\zeta^2)$$

so that, by substituting in (71), and using  $\boldsymbol{\mu}^{(0)} = h \boldsymbol{\mu}_0$  and  $\boldsymbol{\mu}^{(1)} = \frac{h^3}{12} \boldsymbol{\mu}_1$  we obtain

$$\boldsymbol{\mu}_0 = \partial_c \widehat{\psi}(\mathbf{F}, c_0) + \frac{h^2}{24} \partial_c^3 \widehat{\psi}(\mathbf{F}, c_0) c_1^2 + \Omega p_0, \tag{72a}$$

$$\boldsymbol{\mu}_1 = \partial_c^2 \widehat{\psi}(\mathbf{F}, c_0) c_1 + \Omega p_1. \tag{72b}$$

### 5.2. The Flory-Rehner free energy

We assume that the reference configuration  $\mathcal{B}$  of the polymer gel is attained through a homogeneous swelling from the dry state that produces a spatially-uniform spherical distortion  $\mathbf{F}_\star = \lambda_\star \mathbf{I}$ , with  $\lambda_\star \geq 1$ . Hence, the deformation gradient with respect to the dry state and the polymer volume fraction in the current configuration are given by, respectively,

$$\mathbf{F}_d = \lambda_\star \mathbf{F} \quad \text{and} \quad \phi = 1 / (J_\star \det \mathbf{F}), \tag{73}$$

where  $J_\star = \det \mathbf{F}_\star$  and in the computation of  $\phi$  we have assumed that the polymer network is incompressible. According to Gaussian network theory, the strain energy per unit *dry volume* is (e.g. [33], Eq. (3.8))

$$\tilde{\psi}_s(\mathbf{F}_d) = \frac{G}{2} \left( \left| \mathbf{F}_d \right|^2 - 3 \right), \tag{74}$$

where  $G$  is the shear modulus of the polymer network. Thus, the function

$$\widehat{\psi}_s(\mathbf{F}) = \frac{1}{J_\star} \tilde{\psi}_s(\lambda_\star \mathbf{F}) = \frac{G}{2J_\star} \left( \left| \lambda_\star \mathbf{F} \right|^2 - 3 \right) \tag{75}$$

yields the dependence on  $\mathbf{F}$  of the strain energy per unit *reference volume*. Moreover, for  $\chi$  the solvent-polymer interaction parameter, the function (see [33], Eq. (3.68))

$$\tilde{\psi}_m(\phi) = \frac{\mathcal{R}T}{\Omega} \left( \frac{1}{\phi} - 1 \right) (\log(1 - \phi) + \chi \phi)$$

accounts for the mixing energy per unit *dry volume* according to the Flory-Huggins solution theory. Now, given that the amount of solvent per unit dry volume is  $J_\star c$ , the volume fraction in the current configuration is  $\phi = 1 / (1 + \Omega J_\star c)$ . Accordingly, given the volume constraint (46) and (73)<sub>2</sub>, the initial solvent concentration per unit

reference volume is  $c_\star = (J_\star - 1)/\Omega J_\star$ . Moreover,

$$\begin{aligned} \widehat{\psi}_m(c) &= \frac{1}{J_\star} \widehat{\psi}_m \left( \frac{1}{1 + \Omega J_\star c} \right) \\ &= \mathcal{R}Tc \left[ \log \left( \frac{\Omega J_\star c}{1 + \Omega J_\star c} \right) + \chi \frac{1}{1 + \Omega J_\star c} \right] \end{aligned} \quad (76)$$

is the mixing energy per unit reference volume. Summing up,

$$\widehat{\psi}(\mathbf{F}, c) = \widehat{\psi}_s(\mathbf{F}) + \widehat{\psi}_m(c) \quad (77)$$

represents the total Flory-Rehner free energy per unit reference volume.

Now, starting from the general constitutive prescriptions (64), on using the specialization (77) and (75), and on retaining terms up to  $O(h^3)$  we obtain:

$$\mathbf{s}^{(0)} = h \frac{G}{\lambda_\star} \left( \widehat{\mathbf{F}} + \frac{h^2}{24} (\mathbf{d} \otimes \nabla_s \delta + \delta \nabla_s \mathbf{d}) \right) - \mathbf{s}_p^{(0)}, \quad (78a)$$

$$\mathbf{s}^{(1)} = \frac{h^3}{12} \frac{G}{\lambda_\star} \nabla_s \mathbf{d} - \mathbf{s}_p^{(1)}, \quad (78b)$$

$$\mathbf{s}^{(2)} = \frac{h^3}{12} \frac{G}{\lambda_\star} \widehat{\mathbf{F}} - \mathbf{s}_p^{(2)}, \quad (78c)$$

$$\mathbf{s}^{(0)} = h \frac{G}{\lambda_\star} \mathbf{d} - \mathbf{s}_p^{(0)}, \quad (78d)$$

$$\mathbf{s}^{(1)} = \frac{h^3}{12} \frac{G}{\lambda_\star} \delta \mathbf{d} - \mathbf{s}_p^{(1)}, \quad (78e)$$

We next turn to the constitutive equation (72) which, granted (77), become

$$\mu_0 = \partial_c \widehat{\psi}_m(c_0) + \frac{h^2}{24} \partial_c^3 \widehat{\psi}_m(c_0) c_1^2 + \Omega p_0, \quad (79a)$$

$$\mu_1 = \partial_c^2 \widehat{\psi}_m(c_0) c_1 + \Omega p_1, \quad (79b)$$

with

$$\partial_c \widehat{\psi}_m(c_0) = \mathcal{R}T \left( \log \frac{J_\star \Omega c_0}{1 + J_\star \Omega c_0} + \frac{1}{1 + J_\star \Omega c_0} + \frac{\chi}{(1 + J_\star \Omega c_0)^2} \right), \quad (80a)$$

$$\partial_c^2 \widehat{\psi}_m(c_0) = \frac{\mathcal{R}T}{c_0} \frac{1 + J_\star \Omega c_0 (1 - 2\chi)}{(1 + J_\star \Omega c_0)^3}, \quad (80b)$$

$$\partial_c^3 \widehat{\psi}_m(c_0) = -\frac{\mathcal{R}T}{c_0^2} \frac{1 + 4J_\star \Omega c_0 + 3J_\star^2 \Omega^2 c_0^2 (1 - 2\chi)}{(1 + J_\star \Omega c_0)^4}. \quad (80c)$$

### 6. Applications

In this section, we validate numerically the procedure of dimensional reduction by comparing the results obtained with the plate theory with those obtained with the three-dimensional model with reference to three benchmark problems, solved using the finite element method. The three-dimensional model and the related numerical aspects have been described in Ref. [8]. For the reader's sake we provide in Table 1 below a summary of the initial-boundary value problem that arises from our theory.

In what follows, the gel is supposed to be in equilibrium with a solvent at chemical potential  $\mu_e$ . The condition of chemical equilibrium  $\mu_0 = \mu_e, \mu_1 = 0$  is prescribed through a couple of Lagrange multipliers that enter the balance of solvent mass for  $c_0$  and  $c_1$  as bulk source terms in the way illustrated in the remark at the end of Section 3.

#### 6.1. Bending of a cantilever plate

The first problem regards the bending of a cantilever square plate with side length  $L$ , subject to a vertical edge load  $\mathbf{t}^{(0)} = -a\mathbf{e}_2, a > 0$  applied on the edge opposite to the clamp. The chemical potential  $\mu_e$  of the external solvent is kept fixed to the value, determined by the parameters  $G\Omega/\mathcal{R}T = 0.001, \lambda_\star c_\star = 1.5, \chi = 0.2$ , which guarantees that the unloaded configuration of the plate is stress-free. As reported in Fig. 1, the maximum deflection computed using the plate model excellently agrees with that computed using the three-dimensional model, for all the thickness-to-edge ratios  $h/L$  and vertical loads considered. In particular, we notice that the model is able to capture large displacements corresponding to the case  $h/L = 0.01$  at large vertical loads. We also notice that the 6-parameter shell model, where  $\delta \equiv 0$ , significantly

close up space

**Table 1** Data, unknowns, and governing equations of the boundary-value problem arising from our plate theory. The problem is formulated in a space–time domain  $\mathcal{M} \times \mathcal{I}$ , with  $\mathcal{M}$  a two–dimensional region and  $\mathcal{I}$  a time interval.

Unknowns	Primary configuration fields $r, \mathbf{d}, \delta$ concentration fields $c_0$ and $c_1$ pressure fields $p_0, p_1$	Secondary stress resultants $\mathbf{N}, \mathbf{M}, \mathbf{q}, \boldsymbol{\tau}, \boldsymbol{\tau}$ chemical potentials $\mu_0, \mu_1$ fluxes $\mathbf{h}^{(0)}, \mathbf{h}^{(1)}, h_3^{(0)}$
Equations	<b>Balance &amp; constraint</b> balance of forces (26) balance of solvent mass (45) swelling constraint (50)	<b>Constitutive</b> constitutive equations (22), (69) and (78), for the stress resultants constitutive equation (67) for the solvent flux constitutive equation (79) for the chemical potential
Prescribed fields	Bulk load resultants $\mathbf{f}^{(0)}, \bar{\mathbf{f}}^{(1)}, f_d^{(2)}$ on $\mathcal{M} \times \mathcal{I}$ ; Boundary loads $\mathbf{t}^{(0)}, \bar{\mathbf{t}}^{(1)}, t_d^{(2)}$ on $\partial_m^0 \mathcal{M} \times \mathcal{I}$ ; Constraints on the configuration fields $r, \mathbf{d}, \delta$ on $\partial_m^1 \mathcal{M} \times \mathcal{I}$ ; Boundary fluxes $\beta^{(0)}, \beta^{(1)}$ on $\partial_c^0 \mathcal{M} \times \mathcal{I}$ and $\bar{\beta}^{(0)}, \bar{\beta}^{(1)}$ on $\mathcal{M} \times \mathcal{I}$ ; Constraints on the chemical potential fields $\mu_0, \mu_1$ on $\partial_c^1 \mathcal{M} \times \mathcal{I}$ ; Initial conditions for $c_0$ and $c_1$ on $\mathcal{M} \times \{0\}$ .	



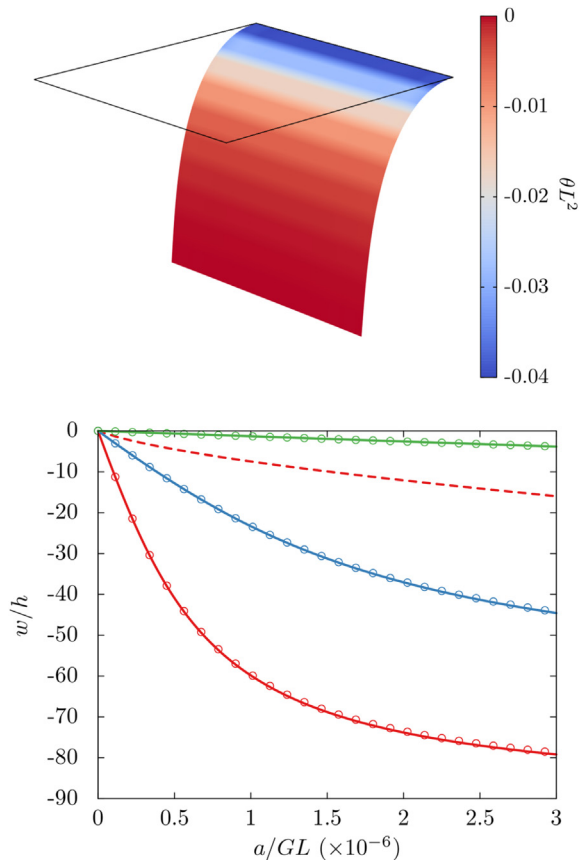


**Fig. 1.** Bending of a square polymer gel plate induced by a vertical edge load with magnitude  $a$  applied far from the clamp: comparison between the plate model and the 3D model, for  $G\Omega/\mathcal{R}T = 0.001$ ,  $\lambda_\star = 1.5$ ,  $\chi = 0.2$ . (Top) Deformed equilibrium shape obtained with the plate model for  $h/L = 0.01$  and  $a/GL = 3 \times 10^{-6}$ . The color code represents the dimensionless curvature  $\theta L^2$  of the midplane, while the black line represents the undeformed configuration of the midplane. (Bottom) Dimensionless vertical displacement  $w/h$  at the tip of the plate as a function of the magnitude of the edge load, for different values of the thickness-to-edge ratio  $h/L$ : 0.01 (red), 0.014 (blue), 0.03 (green). Solid lines are the results obtained with the 3D model, while circles are the results obtained with the plate model. The dashed line corresponds to the 6-parameter model. (For interpretation of the references to colour in this figure legend, the reader is referred to the web version of this article.)

underestimates the deformation of the shell, as observed previously in Ref. [1].

## 6.2. Swelling-induced wrinkling

The second problem regards the swelling-induced wrinkling of a square polymer gel plate pre-stretched between clamps. A similar problem has been studied in Ref. [34]. First, the clamp-to-clamp distance is increased to fix the nominal strain  $\epsilon = (L' - L)/L$ , where  $L'$  is the deformed distance, while keeping the chemical potential of the solvent surrounding the plate unchanged, as in the previous example. We consider nominal strains up to 100%, where the large-strain constitutive equations for the plate are crucial to accurately evaluate the initial membranal stress field. At the end of the pre-stretch phase, the plate contracts laterally without developing wrinkles. Then, the chemical potential of the external solvent is increased up to  $\mu_e/\mathcal{R}T = 0$ , which is higher than the initial chemical potential; as result, the plate absorbs solvent and swells. The constraint imposed by the clamps hampers lateral swelling and thus induces transverse compressive stresses, which trigger the wrinkling instability, as shown in the equilibrium shape of the

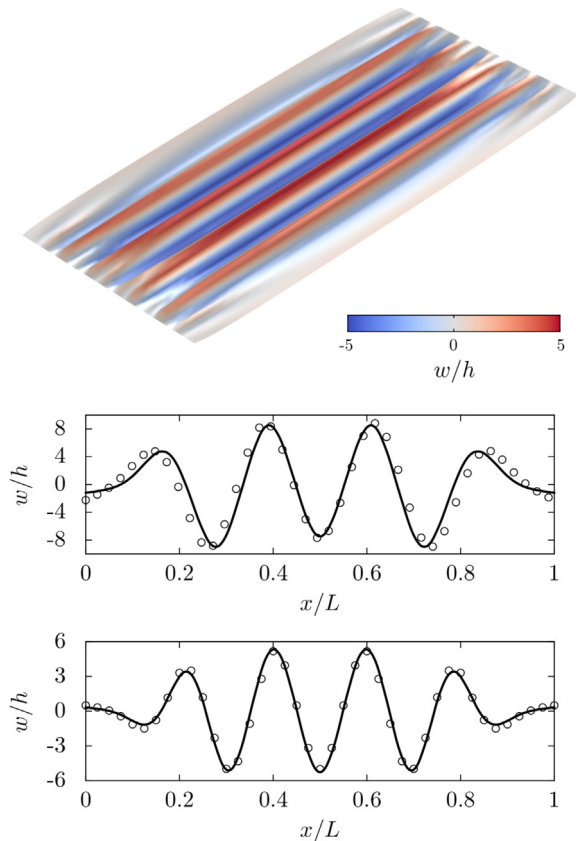


**Fig. 2.** Swelling-induced wrinkling of a square polymer gel plate stretched between clamps: comparison between the plate model and the 3D model, for  $G\Omega/\mathcal{R}T = 0.001$ ,  $\lambda_\star = 1.5$ ,  $\chi = 0.6$ ,  $h/L = 0.001$  and  $\mu_e/\mathcal{R}T = 0$ . (Top) Deformed equilibrium shape obtained with the plate model for the applied strain  $\epsilon = 1.0$ . The color code represents the dimensionless vertical displacement of the midplane. (Bottom) Dimensionless vertical displacement  $w/h$  along the line  $x/L = 1/2$  as a function of the dimensionless transverse coordinate  $y/L$ , for  $\epsilon = 0.5$  (top) and  $\epsilon = 1.0$  (bottom). Solid lines and circles are the results obtained with the 3D model and the plate model, respectively.

wrinkled plate depicted in Fig. 2. Compared to the three-dimensional model, the plate model accurately captures amplitude and wavelength of the equilibrium wrinkling pattern, both decreasing with the nominal strain, in agreement with experimental observations.

## 6.3. Polymer gel composite plates

Inspired by the natural world, where plants adjust their shape by exploiting local changes in swelling, several approaches to shape morphing of polymer gel plates have been proposed. These approaches typically involve the fabrication of polymer gel composite plates [35], either through the embedding of appropriately oriented reinforcing fibers [36,37], or by introducing a spatial modulation of the cross-linking density of the polymer matrix [22–24]. In-plane stresses arising from non-homogeneous swelling drive the transformation of the initial, flat configuration into complex, three-dimensional shapes.

Here, we study a problem similar to that presented in Ref. [38]. We consider a circular plate consisting of an inner disk with radius  $R_i$  and a circular annulus with external radius  $R_e$ . The disk and the annulus are made of two polymeric materials with different shear moduli  $G_i$  and  $G_e$ , respectively, obtained by varying the cross-linking density. We fix the geometrical ratios of the structure as  $R_i/R_e = 3/10$ ,  $R_e/h = 20$ , and the solvent-polymer interaction

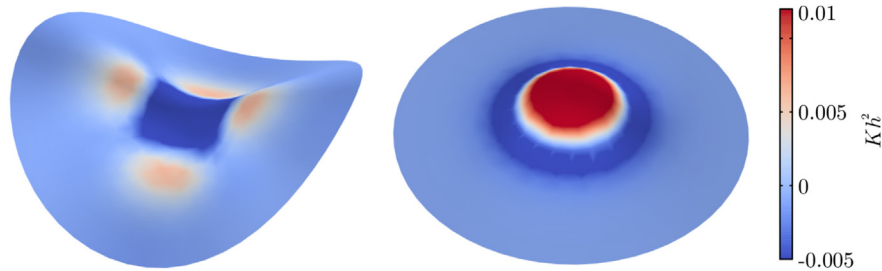


**Fig. 3.** Swelling-induced morphing of saddle-like and hat-like shapes. Deformed equilibrium shapes obtained with the plate model for  $G_i/G_e = 3$  (left) and  $G_i/G_e = 1/3$  (right). The color code represents the dimensionless Gaussian curvature  $Kh^2$  of the midplane. (For interpretation of the references to colour in this figure legend, the reader is referred to the web version of this article.)

parameter as  $\chi = 0.2$ . The initial swelling of the stiff and soft materials is determined by the swelling ratio  $\lambda_\star \approx 1.8$ . Upon increasing the chemical potential of the external solvent up to  $\mu_e/\mathcal{R}T = 0$ , incompatible, differential swelling of the disk and the annulus associated with their non-homogeneous stiffness induces compressive stresses that are relieved by out-of-plane buckling.

In the case of stiffer inner disk, the mid-surface of the plate transforms into a saddle-like surface, while in the case of stiffer annulus a hat-like structure is formed, as reported in Fig. 3. As expected, the Gaussian curvature  $K = \det \nabla_s \mathbf{n}(s) / \det \mathbf{F}$  of the deformed mid-surface is negative (positive) over most of the inner disk in the saddle-like (hat-like) case, while a change in sign of  $K$  occurs across the interface between the disk and the annulus.

## 7. Conclusions

Starting from three-dimensional poroelasticity we have derived a novel fully–nonlinear plate theory describing transient swelling of a thin slab made of an incompressible elastic solid permeated by an incompressible fluid. We have specialized our theory to the case of polymer gels, whose free energy is given by the standard Flory–Rehner expression, and we have implemented the weak formulation of the resulting mathematical model into a finite element code.

Our numerical benchmarks confirm that the theory delivers accurate results, in good agreement with the parent three-dimensional theory. However, since the plate theory is formulated in a two-dimensional domain, its numerical solution is inherently less demanding than that of the full–fledged parent three dimensional theory. This computational efficiency is a desirable feature when dealing with non–linear problems involving bifurcations, such as the swelling-induced wrinkling of a pre-stretched membrane and the shape morphing of composite plates (discussed in Section 6), or with optimization problems for the design and patterning of gel-based composite thin structures.

Differently from existing plate theories for the morphing of thin polymer gels, such as, for instance, those based on the non-Euclidean plate theory [13], our model provides a relation between elastic modulus of the polymer network and swelling, without introducing phenomenological laws derived from the fitting of experimental data. As a result, our model can be used as a predictive tool to study swelling-induced deformations of composite gel plates, with minimal input needed from experiments for the calibration of model parameters.

As we have seen in Section 6, in order to fully exploit the flexibility and accuracy of our model, numerical methods are usually required. Yet, this model can serve as starting point to derive simplified theories with a reduced number of degrees of freedom, to be used in specific applications. For example, in bending-dominated problems involving thin plates free from loads or constraints (*i.e.* the benchmark presented in Section 6.3), small strain

(superimposed to the free swelling in-plane stretches) and plane stress hypotheses are usually appropriate. These hypotheses, together with scaling assumptions on the components of the displacement field, may lead to more treatable models from the analytical viewpoint, such as Föppl–von Kármán plate theories. Nevertheless, we expect the present model to perform well even for moderately thick plates, where the unshearability hypothesis may need to be relaxed, and for problems involving large in-plane forces (*i.e.* the benchmark presented in Section 6.2), where constitutive non-linearities are relevant.

## Acknowledgments

A.L. and A.D.S. acknowledge support from the European Research Council (AdG–340685 – MicroMotility). G.T. acknowledges support from INdAM–GNFM through the initiative “Progetto Giovani”.

## References

- [1] Braun M, Bischoff M, Ramm E. Nonlinear shell formulations for complete three-dimensional constitutive laws including composites and laminates. *Comput Mech* 1994;15(1):1–18. <http://dx.doi.org/10.1007/BF00350285>. URL, <http://link.springer.com/article/10.1007/BF00350285>.
- [2] Sansour C. A theory and finite element formulation of shells at finite deformations involving thickness change: circumventing the use of a rotation tensor. *Arch Appl Mech* 1995;65(3):194–216. <http://dx.doi.org/10.1007/BF00799298>. URL, <http://link.springer.com/article/10.1007/BF00799298>.
- [3] Basar Y, Ding Y. Finite-element analysis of hyperelastic thin shells with large strains. *Comput Mech* 1996;18(3):200–14. <http://dx.doi.org/10.1007/BF00369938>. URL, <http://link.springer.com/article/10.1007/BF00369938>.
- [4] Basar Y, Ding Y. Shear deformation models for large-strain shell analysis. *Int J Solids Struct* 1997;34(14):1687–708. [http://dx.doi.org/10.1016/S0020-7683\(96\)00121-7](http://dx.doi.org/10.1016/S0020-7683(96)00121-7). URL, <http://www.sciencedirect.com/science/article/pii/S0020768396001217>.
- [5] Sussman T, Bathe K-J. 3d-shell elements for structures in large strains. *Comput Struct* 2013;122:2–12. <http://dx.doi.org/10.1016/j.compstruc.2012.12.018>. URL, <http://www.sciencedirect.com/science/article/pii/S004579491200332X>.
- [6] Hong W, Zhao X, Zhou J, Suo Z. A theory of coupled diffusion and large deformation in polymeric gels. *J Mech Phys Solids* 2008;56(5):1779–93. <http://dx.doi.org/10.1016/j.jmps.2007.11.010>. URL, <http://linkinghub.elsevier.com/retrieve/pii/S0022509607002244>.
- [7] Wang X, Hong W. A visco-poroelastic theory for polymeric gels. *P Roy Soc Lond A Mat* 2012;468(2148):3824–41. <http://dx.doi.org/10.1098/rspa.2012.0385>. URL, <http://rspa.royalsocietypublishing.org/cgi/doi/10.1098/rspa.2012.0385>.
- [8] Lucantonio A, Nardinocchi P, Teresi L. Transient analysis of swelling-induced large deformations in polymer gels. *J Mech Phys Solids* 2013;61:205–18. <http://dx.doi.org/10.1016/j.jmps.2012.07.010>. URL, <http://www.sciencedirect.com/science/article/pii/S0022509612001548>.
- [9] Zhang J, Zhao X, Suo Z, Jiang H. A finite element method for transient analysis of concurrent large deformation and mass transport in gels. *J Appl Phys* 2009;105(9):093522. <http://dx.doi.org/10.1063/1.3106628>. URL, <http://scitation.aip.org/content/aip/journal/jap/105/9/10.1063/1.3106628>.
- [10] Bouklas N, Landis CM, Huang R. A nonlinear, transient finite element method for coupled solvent diffusion and large deformation of hydrogels. *J Mech Phys Solids* 2015;79:21–43. <http://dx.doi.org/10.1016/j.jmps.2015.03.004>. URL, <http://www.sciencedirect.com/science/article/pii/S0022509615000605>.
- [11] Chester SA, Leo CVD, Anand L. A finite element implementation of a coupled

- diffusion-deformation theory for elastomeric gels. *Int J Solids Struct* 2015;52: 1–18. <http://dx.doi.org/10.1016/j.ijsolstr.2014.08.015>. URL, <http://www.sciencedirect.com/science/article/pii/S0020768314003278>.
- [12] Taber LA. A theory for transverse deflection of poroelastic plates. *J Appl Mech* 1992;59(3):628–34. <http://dx.doi.org/10.1115/1.2893770>. URL, <http://appliedmechanics.asmedigitalcollection.asme.org/article.aspx?articleid=1410787>.
- [13] Efrati E, Sharon E, Kupferman R. Elastic theory of unconstrained non-euclidean plates. *J Mech Phys Solids* 2009;57(4):762–75. <http://dx.doi.org/10.1016/j.jmps.2008.12.004>. URL, <http://linkinghub.elsevier.com/retrieve/pii/S0022509608002160>.
- [14] Dervaux J, Ciarletta P, Ben Amar M. Morphogenesis of thin hyperelastic plates: a constitutive theory of biological growth in the föppl–von kármán limit. *J Mech Phys Solids* 2009;57(3):458–71. <http://dx.doi.org/10.1016/j.jmps.2008.11.011>. URL, <http://linkinghub.elsevier.com/retrieve/pii/S0022509608002093>.
- [15] Lewicka M, Mahadevan L, Pakzad MR. The föppl–von kármán equations for plates with incompatible strains. *P Roy Soc Lond A Mat* 2010;467(2126): 402–26. <http://dx.doi.org/10.1098/rspa.2010.0138>. URL, <http://rspa.royalsocietypublishing.org/content/467/2126/402>.
- [16] Goriely A, Ben Amar M. Differential growth and instability in elastic shells. *Phys Rev Lett* 2005;94:198103. <http://dx.doi.org/10.1103/PhysRevLett.94.198103>. URL, <http://link.aps.org/doi/10.1103/PhysRevLett.94.198103>.
- [17] Sharon E, Efrati E. The mechanics of non-euclidean plates. *Soft Matter* 2010;6(22):5693. <http://dx.doi.org/10.1039/c0sm00479k>. URL, <http://xlink.rsc.org/?DOI=c0sm00479k>.
- [18] Dias MA, Hanna JA, Santangelo CD. Programmed buckling by controlled lateral swelling in a thin elastic sheet. *Phys Rev E* 2011;84(3):036603. <http://dx.doi.org/10.1103/PhysRevE.84.036603>. URL, <http://link.aps.org/doi/10.1103/PhysRevE.84.036603>.
- [19] Agostiniani V, DeSimone A. Rigorous derivation of active plate models for thin sheets of nematic elastomers. *arXiv Preprint arXiv:1509.07003*. 2015. URL, <http://arxiv.org/pdf/1509.07003>.
- [20] Agostiniani V, DeSimone A, Koumatos K. Shape programming for narrow ribbons of nematic elastomers. *arXiv Preprint arXiv:1603.02088*. 2016. URL, <http://arxiv.org/pdf/1603.02088>.
- [21] Tomassetti G, Varano V. Capturing the helical to spiral transitions in thin ribbons of nematic elastomers. *arXiv Preprint arXiv:1608.02793*. 2016. URL, <http://arxiv.org/pdf/1608.02793>.
- [22] Klein Y, Efrati E, Sharon E. Shaping of elastic sheets by prescription of non-euclidean metrics. *Science* 2007;315(5815):1116–20. <http://dx.doi.org/10.1126/science.1135994>. URL, <http://www.sciencemag.org/cgi/doi/10.1126/science.1135994>.
- [23] Kim J, Hanna JA, Byun M, Santangelo CD, Hayward RC. Designing responsive buckled surfaces by halftone gel lithography. *Science* 2012;335(6073): 1201–5. <http://dx.doi.org/10.1126/science.1215309>. URL, <http://www.ncbi.nlm.nih.gov/pubmed/22403385>.
- [24] Wu ZL, Moshe M, Greener J, Therien-Aubin H, Nie Z, Sharon E, et al. Three-dimensional shape transformations of hydrogel sheets induced by small-scale modulation of internal stresses. *Nat Commun* 2013;4:1586. <http://dx.doi.org/10.1038/ncomms2549>. URL, <http://www.nature.com/doi/10.1038/ncomms2549>.
- [25] Gemmer J, Venkataramani SC. Shape transitions in hyperbolic non-euclidean plates. *Soft Matter* 2013;9(34):8151–61. URL, <http://xlink.rsc.org/?DOI=c3sm50479d>.
- [26] Noselli G, Lucantonio A, McMeeking RM, DeSimone A. Poroelastic toughening in polymer gels: a theoretical and numerical study. *J Mech Phys Solids* 2016;94:33–46. URL, <http://www.sciencedirect.com/science/article/pii/S0022509616301818>.
- [27] Lucantonio A, Noselli G, Trepax X, DeSimone A, Arroyo M. Hydraulic fracture and toughening of a brittle layer bonded to a hydrogel. *Phys Rev Lett* 2015;115:188105. <http://dx.doi.org/10.1103/PhysRevLett.115.188105>. URL, <http://link.aps.org/doi/10.1103/PhysRevLett.115.188105>.
- [28] A. Lucantonio, G. Noselli, Concurrent factors determine toughening in the hydraulic fracture of poroelastic composites, submitted, 2016.
- [29] Lucantonio A, Teresi L, DeSimone A. Continuum theory of swelling material surfaces with applications to thermo-responsive gels and surface mass transport. *J Mech Phys Solids* 2016;89:96–109. <http://dx.doi.org/10.1016/j.jmps.2016.02.001>. URL, <http://www.sciencedirect.com/science/article/pii/S0022509616300746>.
- [30] Antman SS. *Nonlinear problems of elasticity*. Springer; 2005.
- [31] DiCarlo A, Podio-Guidugli P, Williams W. Shells with thickness distension. *Int J Solids Struct* 2001;38:1201–25. [http://dx.doi.org/10.1016/S0020-7683\(00\)00082-2](http://dx.doi.org/10.1016/S0020-7683(00)00082-2). URL, <http://www.sciencedirect.com/science/article/pii/S002076830000822>.
- [32] Duda FP, Souza AC, Fried E. A theory for species migration in a finitely strained solid with application to polymer network swelling. *J Mech Phys Solids* 2010;58(4):515–29. <http://dx.doi.org/10.1016/j.jmps.2010.01.009>. URL, <http://www.sciencedirect.com/science/article/pii/S0022509610000189>.
- [33] Doi M. Gel dynamics. *J Phys Soc Jpn* 2009;78(5):052001. URL, <http://journals.jps.jp/doi/abs/10.1143/JPSJ.78.052001>.
- [34] Lucantonio A, Roché M, Nardinocchi P, Stone HA. Buckling dynamics of a solvent-stimulated stretched elastomeric sheet. *Soft Matter* 2014;10(16): 2800. <http://dx.doi.org/10.1039/c3sm52941j>. URL, <http://xlink.rsc.org/?DOI=c3sm52941j>.
- [35] Dickey MD. Hydrogel composites: shaped after print. *Nat Mater* 2016;15(4): 379–80. URL, <http://dx.doi.org/10.1038/nmat4608>.
- [36] Erb RM, Sander JS, Grisch R, Studart AR. Self-shaping composites with programmable bioinspired microstructures. *Nat Commun* 2013;4:1712. URL, <http://www.nature.com/doi/10.1038/ncomms2666>.
- [37] Sydney Gladman A, Matsumoto EA, Nuzzo RG, Mahadevan L, Lewis JA. Biomimetic 4d printing. *Nat Mater* 2016;15:413–8. URL, <http://www.nature.com/nmat/journal/vaop/ncurrent/full/nmat4544.html>.
- [38] Pezzulla M, Shillig SA, Nardinocchi P, Holmes DP. Morphing of geometric composites via residual swelling. *Soft Matter* 2015;11(29):5812–20. URL, <http://dx.doi.org/10.1039/C5SM00863H>.